Geochemical Perspectives Letters

© 2017 European Association of Geochemistry

Tracking the formation of magma oceans in the Solar System using stable magnesium isotopes

M. Schiller[1]*, J.A. Dallas[1], J. Creech[2], M. Bizzarro[1], J.A. Baker[3]

OPEN ACCESS

doi: 10.7185/geochemlet.1703

Abstract

The processes associated with magma ocean formation and solidification can control the earliest compositional differentiation and volatile inventory of planetary bodies. Thus, elucidating the scale and extent to which magma oceans existed in the Solar System is critical for a full understanding of planet formation. Here we show that the magnesium isotope compositions of the co-magmatic diogenite and eucrite meteorites originating from the protoplanet Vesta are distinct and this is a predictable consequence of extensive crystallisation in a shallow magma ocean. The enrichment in the heavy magnesium isotopes observed in eucrites relative to diogenites is consistent with the isotopic differences measured between minerals and whole-rock basalts on Earth and other asteroids. This isotope effect is not readily observed on Earth due to the lower primary melt magnesium contents produced at smaller degrees of melting and less extensive amounts of mafic mineral crystallisation. However, it is discernible on other planetary bodies where magma oceans formed and crystallised and, thus, Mg isotopes provide a tracer of their previous existence.

Received 1 June 2016 | Accepted 15 August 2016 | Published 1 September 2016

Introduction

Magma oceans are widely considered to have existed on planetary bodies in the early Solar System, given the monominerallic nature of much of the lunar crust (Wood *et al.*, 1970) and extremely ancient ages obtained for lunar, martian and asteroidal igneous rock (*e.g.*, Debaille *et al.*, 2007; Nemchin *et al.*, 2009; Schiller *et al.* 2011). These may have been produced by planetary scale melting induced by heating of short-lived ^{26}Al in the case of early-formed protoplanets such as

1. Centre for Star and Planet Formation, University of Copenhagen, *Øster* Voldgade 5–7, 1350 Copenhagen, Denmark
* Corresponding author (email: schiller@snm.ku.dk)
2. Institut de Physique du Globe de Paris, Université Paris Diderot, CNRS UMR 7154, 75005 Paris, France
3. School of Environment, The University of Auckland, Private Bag 92019, Auckland, New Zealand

Vesta (Greenwood *et al.*, 2005), or giant impacts such as the Moon-forming event in the case of the Earth and Moon (Tonks and Melosh, 1993). As such, finding robust geochemical fingerprints of these ancient magma oceans is important for understanding the earliest stages of planetary evolution.

A range of newly developed stable isotope systems are yielding novel insights into planetary accretion, differentiation and evolution (*e.g.*, Greenwood *et al.*, 2005; Georg *et al.*, 2007). However, many of these systems are multiply affected by a range of processes, potentially including core formation and crystallisation of accessory minerals, which makes interpretation of such data challenging. The lithophile, major element magnesium (Mg) is almost unique in this regard, as stable isotope fractionation in magmatic systems will be almost entirely controlled by crystallisation of high-Mg, mafic minerals, assuming isotopic fractionations exist between such minerals and magma.

The large degree of planetary melting required to generate a magma ocean would produce highly magnesian magmas, which would then subsequently crystallise large amounts of mafic, Mg-rich minerals such as olivine. Small Mg stable isotope fractionations exist between co-existing terrestrial mantle olivine, orthopyroxene and clinopyroxene, with olivine being the isotopically lightest phase (Handler *et al.*, 2009; Young *et al.*, 2009; Pogge von Strandmann *et al.*, 2011; Xiao *et al.*, 2013). Consequently, it should also be possible to detect progressive Mg isotope changes in the products of a crystallising magma ocean.

Vesta is the second largest asteroid in the Solar System and comprises a metal core, silicate mantle and crust (Russell *et al.*, 2012). Based on spectral observations and the Dawn Mission, the howardite–eucrite–diogenite (HED) meteorite suite is inferred to come from Vesta (McCord *et al.*, 1970; Binzel and Xu, 1993; Russell *et al.*, 2012). Most HED meteorites also share common nucleosynthetic isotope signatures for some elements that demonstrate their genetic affinity (Greenwood *et al.*, 2005). These lithologically diverse meteorites provide a unique archive of the timing and processes of protoplanet formation and differentiation. Diogenites are mostly orthopyroxenites, and are conventionally viewed as cumulate igneous rocks formed in a magma ocean or bodies on Vesta, whereas eucrites are basaltic and gabbroic rocks predominantly composed of pigeonite and plagioclase (Mittlefehldt, 2014).

Despite many decades of petrological, geochemical and chronological study, the petrogenesis of eucrites and diogenites and the relationship between them remain enigmatic. End-member models include limited partial melting or extensive (*i.e.* magma ocean) melting of Vesta (Stolper, 1977; Mandler and Elkins-Tanton, 2013; Mittlefehldt, 2014). Nearly all models are difficult to reconcile with the large range of incompatible trace element concentrations in diogenites and eucrites. However, a recent study by Mandler and Elkins-Tanton (2013) has used both chemical and physical arguments to create a model that links HED lithologies to different stages of a differentiating global-scale magma ocean.

Mg Isotope Evidence for a Vestan Magma Ocean

Insights into the degree of partial melting on Vesta can be gleaned from the major and trace element chemistry of the most primitive, oldest diogenites that have the largest deficits in radiogenic ^{26}Mg (Schiller *et al.*, 2011) and features indicating crystallisation from melts with broadly chondritic rare earth element ratios (the full methodological approach is described in the Supplementary Information). Our modelling (Fig. 1) shows that diogenites crystallised as cumulates from >50 % partial melt of a chondritic precursor. This melt would have been part of either a global magma ocean (Mandler and Elkins-Tanton, 2013) or, given thermal modelling constraints, a more localised shallow magma ocean (Neumann *et al.*, 2014). The diogenite parental magmas produced by such large degrees of melting of the vestan, post-core, silicate mantle are highly magnesian with *ca*. 19–33 wt. % MgO (*e.g.*, Ashcroft and Wood, 2015) and would undergo *ca*. >50 %–70 % olivine and orthopyroxene crystallisation before the MgO content of the residual melt approaches that of eucrites. A stable Mg isotopic difference should exist between diogenites and eucrites if they are genetically related by large amounts of olivine and orthopyroxene crystallisation, and if there is a small isotopic fractionation between olivine–orthopyroxene and melt.

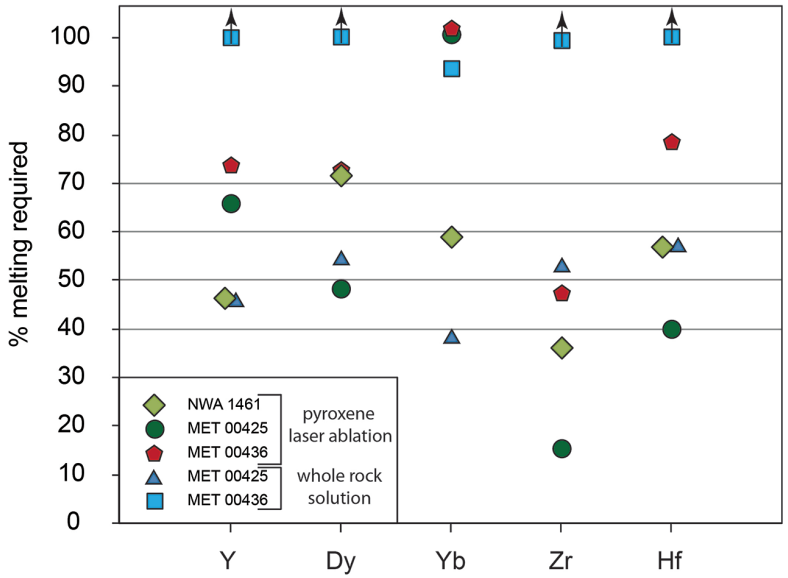

Figure 1 The minimum degree of partial melting of the vestan mantle, based on modelling the selected incompatible trace element contents of primitive diogenites. Calculations are based on trace element data for pyroxene determined by laser ablation ICP-MS (Schiller *et al.*, 2011) or digestions of leached whole rock diogenites measured by solution ICP-MS (Barrat *et al.*, 2010). Details of the partial melting model can be found in the Supplementary Information.

We present high-precision stable Mg isotope data for 22 eucrites determined by multiple-collector inductively coupled plasma mass spectrometry using well established analytical protocols (Table 1; see Supplementary Information for more details) and compare these with published (n = 23) and new (n = 2) values for 25 diogenites obtained with exactly the same analytical methods (Schiller *et al.*, 2011 and this study). The mean Mg stable isotope composition

Table 1 Mg stable isotope data for 22 eucrites, 2 diogenites and the terrestrial basalt standard BHVO-2 relative to the Mg standard DSM-3.

Sample	μ^{25}Mg (±2 SE; ppm)	μ^{26}Mg (±2 SE; ppm)
Terrestrial basalt		
BHVO-2	–133 ± 20	–252 ± 38
Polymict eucrites		
EET 83227	–105 ± 6	–180 ± 10
Mg-rich eucrites		
EET 87548	–104 ± 25	–192 ± 47
LEW 87002	–37 ± 14	–65 ± 30
Brecciated eucrites		
Camel Donga	+33 ± 21	+111 ± 43
EET 92003	–41 ± 12	–52 ± 24
GRA 98006	–67 ± 10	–88 ± 18
GRA 98033	–83 ± 13	–124 ± 25
GRA 98043	–63 ± 14	–89 ± 27
GRA 98055	–70 ± 25	–89 ± 49
GRA 98114	–83 ± 18	–111 ± 36
GRO 95533	–54 ± 13	–61 ± 25
Juvinas	–106 ± 4	–174 ± 7
LAP 031062	–60 ± 12	–96 ± 24
LAR 06875	–34 ± 17	–26 ± 32
Millibillilie	–60 ± 28	–76 ± 65
PCA 91193	–66 ± 18	–109 ± 35
QUE 99005	–62 ± 11	–81 ± 21
RKPA 80204	–66 ± 9	–93 ± 17
SCO 06041	–21 ± 11	–29 ± 20
Unbrecciated eucrites		
EET 92023	–96 ± 5	–156 ± 11
LEW 85035	–65 ± 17	–91 ± 33
QUE 97014	–55 ± 14	–74 ± 28
Diogenites		
Dhofar 700	–125 ± 3	–212 ± 8
NWA 4215	–112 ± 16	–212 ± 32

for 22 eucrites is $\mu^{25}Mg_{DSM-3} = -62 \pm 13$ ppm (2 SE; Fig. 2), which is heavier than the mean of diogenites [$\mu^{25}Mg_{DSM-3} = -118 \pm 11$ ppm (2 SE)]. A t-test shows that the isotopic difference between eucrites and diogenites is statistically significant ($p = 5.5 \times 10^{-8}$). Diogenites have stable Mg isotopes that are indistinguishable from those for Earth's mantle and chondrite meteorites, although within the heavier range for these materials. In contrast, eucrites are isotopically heavier than all these materials (Fig. 2).

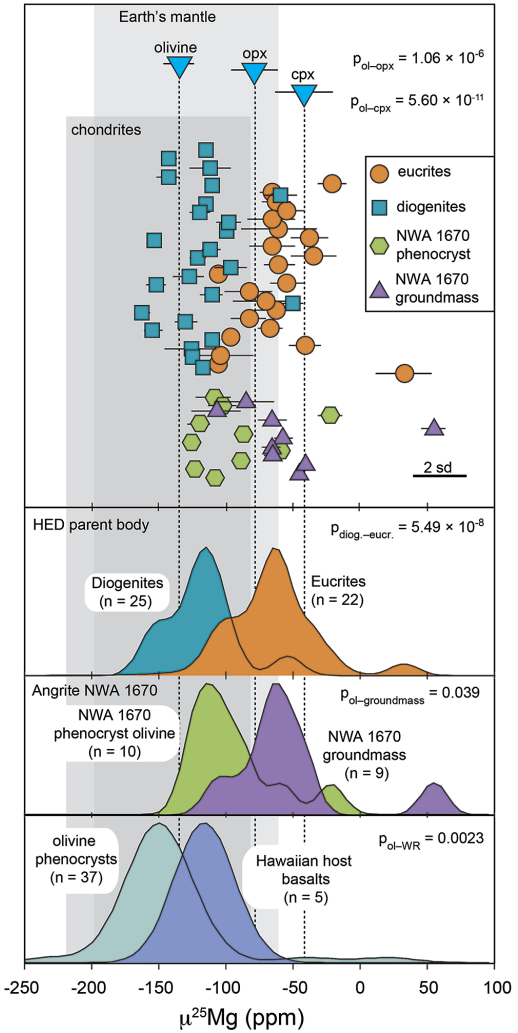

Figure 2 Stable Mg isotope composition ($\mu^{25}Mg$, where $\mu^{25}Mg = [(^{25}Mg/^{24}Mg)_{sample} / (^{25}Mg/^{24}Mg)_{DSM-3} - 1] \times 10^6$) of diogenites and eucrites (Schiller *et al.*, 2011 and this study), phenocryst olivine and groundmass from the angrite meteorite NWA 1670 (Schiller *et al.*, 2015), and Hawaiian basalts and olivine phenocrysts least affected by Mg–Fe inter-diffusion based on their Fe stable isotope composition (Teng *et al.*, 2011 and references therein). The bottom of the figure shows the probability density distribution of each group and the results of t-testing. The external reproducibility reported for each respective study or the internal error, whichever was larger, was used for the calculation of the probability density distributions and t-testing. Also shown are the ranges of the Mg stable isotope compositions of Earth's mantle (Teng *et al.*, 2010) and chondrites (Teng *et al.*, 2010; Larsen *et al.*, 2016), as well as the average $\mu^{25}Mg$ of olivine, orthopyroxene and clinopyroxene in Earth's mantle (Handler *et al.*, 2009; Young *et al.*, 2009; Pogge von Strandmann *et al.*, 2011; Xiao *et al.*, 2013).

Before attributing the stable Mg isotope difference between diogenites and eucrites to magmatic processes, it is necessary to consider other processes that might explain this. Firstly, diffusion in magmatic systems can fractionate Mg and iron (Fe) isotopes (Teng *et al.*, 2011), which generates a negative correlation between Mg and Fe stable isotopes, with Fe isotopes being more sensitive to this process than Mg isotopes in Mg-rich olivine. This is inconsistent with the eucrite data, given that eucrites have heavy Mg compared to diogenites but indistinguishable Fe isotope compositions (Wang *et al.*, 2012). Furthermore, diogenites have a light Mg isotope composition when compared to eucrites, which is opposite to the prediction of a heavy Mg isotope composition of olivine and pyroxene resulting from inter-diffusion with a melt (Fig. 2). Secondly, small stable Mg isotope differences exist between mafic minerals (Fig. 2) and, as such, mineralogical differences between diogenites and eucrites might explain their whole-rock stable isotope offset. However, given that low-Ca pyroxene is the dominant host of Mg in both diogenites and eucrites, the isotope offset between eucrites and diogenites is too large to reflect solely mineralogical differences. Thus, we attribute the stable Mg isotope difference between diogenites and eucrites to a magmatic process, whereby extensive fractionation of mafic minerals (olivine and orthopyroxene) with light Mg from a (very) large degree melt of vestan mantle produced progressively heavier Mg isotopes in the residual (eucritic) magma.

A study of basaltic samples from the Kileaua Iki lava lake on Hawaii (Teng *et al.*, 2007) provide a possible upper limit on the $\mu^{25}Mg$ difference between olivine and melt of 35 ppm. The analytical uncertainty of our $\mu^{25}Mg$ measurements and the larger extent of mafic mineral fractionation during magma evolution on Vesta explain why changes in $\mu^{25}Mg$ are detectable in HED meteorites. Further evidence of high-temperature stable Mg isotope fractionation between minerals and melt in different settings is shown in Figure 2. Firstly, Mg-rich olivines and surrounding quenched groundmass in the angrite meteorite NWA 1670 have a statistically significant Mg stable isotopic difference ($\mu^{25}Mg_{melt-olivine} = +42$ ppm; Fig. 2; Schiller *et al.*, 2015). Published data for Hawaiian basalts and their olivine phenocrysts that have stable Fe isotopes least affected by diffusion (*i.e.* heavy olivine Fe isotopes) also have a statistically significant difference in $\mu^{25}Mg$ with $\mu^{25}Mg_{melt-olivine} = +28$ ppm (Fig. 2; Teng *et al.*, 2011 and references therein). As such, we consider that extensive mafic mineral crystallisation from a large degree partial melt represents the most viable explanation for the heavy Mg isotope composition of eucrites and the $\mu^{25}Mg$ offset between diogenites and eucrites.

A simple model for the evolving MgO and $\mu^{25}Mg$ in a magma undergoing olivine and orthopyroxene crystallisation is illustrated in Figure 3. This shows that *ca.* 45 % olivine equilibrium crystallisation and 30 % orthopyroxene fractional crystallisation from a 100 % melt of the vestan silicate mantle will produce a melt residue with MgO (*ca.* 6 wt. %) and $\mu^{25}Mg$ (–64 ppm), which is comparable to that of eucrites. Although mineral–melt equilibrium isotope fractionation at high temperatures is small, only a $\mu^{25}Mg_{melt-olivine} = +35$ ppm and $\mu^{25}Mg_{melt-orthopyroxene} = +20$ ppm would be required to generate this isotopic fractionation (Fig. 3). Alternatively, the data can also be modelled from a parental

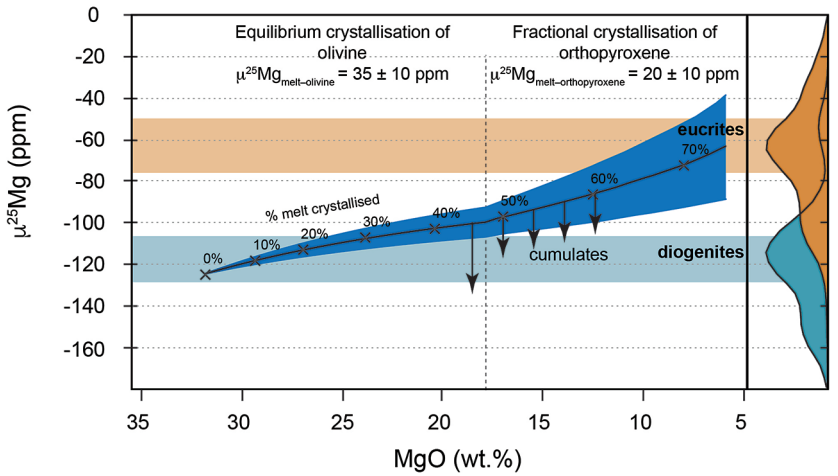

Figure 3 Modelled MgO and stable Mg isotope ($\mu^{25}Mg$) evolution of a 100 % putative primary melt on Vesta (Ashcroft and Wood, 2015) of the post-core formation, vestan silicate mantle (MgO = 31.8 wt. %). Melt–olivine $\mu^{25}Mg$ fractionation of +35 ppm ($\mu^{25}Mg_{melt-olivine}$) and melt–orthopyroxene $\mu^{25}Mg$ fractionation of +20 ppm ($\mu^{25}Mg_{melt-orthopyroxene}$) can generate the heavy stable Mg isotopes ($\mu^{25}Mg$ = –62 ppm) and MgO contents (*ca.* 6 wt. %) of eucrites. Olivine–orthopyroxenite cumulates generated during this process have $\mu^{25}Mg$ values in the range of diogenites.

magma produced by smaller, but still very large, degrees of melting (65 %) that undergoes crystallisation (Fig. S-1b). The lighter Mg isotopic composition of olivine and orthopyroxene as compared with basaltic melt is broadly consistent with stable isotope theory (Wilding *et al.,* 2004; Henderson *et al.,* 2006), given that Mg is in six-fold and five-fold coordination in olivine–orthopyroxene crystals and silicate melts, respectively. Moreover, the high MgO contents of large degree melts of the vestan silicate mantle along with the lower pressure crystallisation on this protoplanet are predicted to result in even lower Mg coordination in vestan silicate melts than terrestrial magmas (Wilding *et al.,* 2004).

Conclusions

Although our results cannot distinguish between a global scale or a shallow magma ocean, we consider a global scale magma ocean to be inconsistent with recent thermal models (Neumann *et al.,* 2014) and other geochemical evidence (Barrat and Yamaguchi, 2014). Irrespective, we have shown that very large degrees of melting characterised at least parts of Vesta and that a co-magmatic relationship broadly exists between diogenites and eucrites. This study also shows that high-temperature, magmatic processes can fractionate stable Mg isotopes in evolving mafic magmas. With the current resolution of analytical techniques,

this isotopic difference is not readily observed in igneous rocks from Earth due to the lower primary melt Mg contents of post-Archean igneous rocks produced at smaller degrees of melting and consequently more limited amounts of olivine crystallisation (Fig. S-1b) relative to Vesta. However, stable Mg isotope fractionations should be discernible on other rocky planets, satellites and asteroids where silicate melting was extensive and magma oceans formed and crystallised.

Acknowledgements

Financial support for this project was provided by the Royal Society of New Zealand's Marsden Fund (JB), the Danish National Research Foundation (DNRF97, MB), and the European Research Council (ERC Consolidator Grant Agreement 616027 —STARDUST2ASTEROIDS, MB). We like to thank R. Carlson and two anonymous reviewers for their constructive comments on this paper. The authors also wish to thank NASA for providing most of the meteorite samples.

Editor: Bruce Watson

Additional Information

Supplementary Information accompanies this letter at www.geochemicalperspectivesletters.org/article1703

Reprints and permission information is available online at http://www.geochemicalperspectivesletters.org/copyright-and-permissions

Cite this letter as: Schiller, M., Dallas, J.A., Creech, J., Bizzarro, M., Baker, J.A. (2017) Tracking the formation of magma oceans in the Solar System using stable magnesium isotopes. *Geochem. Persp. Let.* 3, 22-31.

References

Ashcroft, H.O., Wood, B.J. (2015) An experimental study of partial melting and fractional crystallisation on the HED parent body. *Meteoritics and Planetary Science* 48, 2333–2349.

Barrat, J.A., Yamaguchi, A. (2014) Comment on "The origin of eucrites, diogenites, and olivine diogenites: Magma ocean crystallisation and shallow magma processes on Vesta" by B.E. Mandler and L.T. Elkins-Tanton. *Meteoritics and Planetary Science* 49, 468–472.

Barrat, J.A., Yamaguchi, A., Zanda, B., Bollinger, C., Bohn, M. (2010) Relative chronology of crust formation on asteroid Vesta: Insights from the geochemistry of diogenites. *Geochimica et Cosmochimica Acta* 74, 6218–6231.

Binzel, R.P., Xu, S. (1993) Chips off of asteroid 4 Vesta: Evidence for the parent body of basaltic achondrite meteorites. *Science* 260, 186–191.

Debaille, V., Brandon, A.D., Yin, Q.Z., Jacobsen, B. (2007) Coupled ^{142}Nd–^{143}Nd evidence for a protracted magma ocean in Mars. *Nature,* 450, 525–528.

GEORG, R.B., HALLIDAY, A.N., SCHAUBLE, E.A., REYNOLDS, B.C. (2007) Silicon in the Earth's core. *Nature* 447, 1102–1106.

GREENWOOD, R.C., FRANCHI, I.A., JAMBON, A., BUCHANAN, P.C. (2005) Widespread magma oceans on asteroidal bodies in the early Solar System. *Nature* 435, 916–918.

HANDLER, M.R., BAKER, J.A., SCHILLER, M., BENNETT, V.C., YAXLEY, G.M. (2009) Magnesium stable isotope composition of Earth's upper mantle. *Earth and Planetary Science Letters* 282, 306–313.

HENDERSON, G.S., CALAS, G., STEBBINS, J.F. (2006) The structure of silicate glasses and melts. *Elements* 2, 269–273.

LARSEN, K.K., SCHILLER, M., BIZZARRO, M. (2016) Accretion timescales and style of asteroidal differentiation in an ^{26}Al-poor protoplanetary disk. *Geochimica et Cosmochimica Acta* 176, 295–315.

MANDLER, B.E., ELKINS-TANTON, L.T. (2013) The origin of eucrites, diogenites, and olivine diogenites: Magma ocean crystallisation and shallow magma chamber processes on Vesta. *Meteoritics and Planetary Science* 48, 2333–2349.

MCCORD, T.B., ADAMS, J.B., JOHNSON, T.V. (1970) Asteroid Vesta: Spectral reflectivity and compositional implications. *Science* 168, 1445–1447.

MITTLEFEHLDT, D.W. (2014) Asteroid (4) Vesta: I. The howardite–eucrite–diogenite (HED) clan of meteorites. *Chemie der Erde – Geochemistry* 75, 155–183.

NEMCHIN, A., TIMMS, N., PIDGEON, R., GEISLER, T., REDDY, S., MEYER, C. (2009) Timing of crystallisation of the lunar magma ocean constrained by the oldest zircon. *Nature Geoscience* 2, 133–136.

NEUMANN, W., BREUER, D., SPOHN, T. (2014) Differentiation of Vesta: Implications for a shallow magma ocean. *Earth and Planetary Science Letters* 395, 267–280.

POGGE VON STRANDMANN, P.A.E., ELLIOTT, T., MARSCHALL, H.R., COATH, C., LAI, Y.-J., JEFFCOATE, A.B., IONOV, D.A. (2011) Variations of Li and Mg isotope ratios in bulk chondrites and mantle xenoliths. *Geochimica et Cosmochimica Acta* 75, 5247–5268.

RUSSELL, C.T., RAYMOND, C.A., CORADINI, A., MCSWEEN, H.Y., ZUBER, M.T., NATHUES, A., DE SANCTIS, M.C., JAUMANN, R., KONOPLIV, A.S., PREUSKER, F., ASMAR, S.W., PARK, R.S., GASKELL, R., KELLER, H.U., MOTTOLA, S., ROATSCH, T., SCULLY, J.E.C., SMITH, D.E., TRICARICO, P., TOPLIS, M.J., CHRISTENSEN, U.R., FELDMAN, W.C., LAWRENCE, D.J., MCCOY, T.J., PRETTYMAN, T.H., REEDY, R.C., SYKES, M.E., TITUS, T.N. (2012) Dawn at Vesta: Testing the protoplanetary paradigm. *Science* 336, 684–686.

SCHILLER, M., BAKER, J.A., CREECH, J., PATON, C., MILLET, M.-A., IRVING, A., BIZZARRO, M. (2011) Rapid timescales for magma ocean crystallisation on the howardite–eucrite–diogenite parent body. *Astrophysical Journal Letters* 740, L22.

SCHILLER, M., CONNELLY, J.N., GLAD, A.C., MIKOUCHI, T., BIZZARRO, M. (2015) Early accretion of protoplanets inferred from a reduced inner solar system ^{26}Al inventory. *Earth and Planetary Science Letters* 420, 45–54.

STOLPER, E. (1977) Experimental petrology of eucritic meteorites. *Geochimica et Cosmochimica Acta* 41, 587–611.

TENG, F.-Z., WADHWA, M., HELZ, R.T. (2007) Investigation of magnesium isotope fractionation during basalt differentiation: Implications for a chondritic composition of the terrestrial mantle *Earth and Planetary Science Letters* 261, 84–92.

TENG, F.-Z., LI, W.-Y., KE, S., MARTY, B., DAUPHAS, N., HUANG, S., WU, F.-Y., POURMAND, A. (2010) Magnesium isotopic composition of the Earth and chondrites. *Geochimica et Cosmochimica Acta* 74, 4150–4166.

TENG, F.-Z., DAUPHAS, N., HELZ, R.T., GAO, S., HUANG, S. (2011) Diffusion-driven magnesium and iron isotope fractionation in Hawaiian olivine. *Earth and Planetary Science Letters* 308, 317–324.

TONKS, W.B., MELOSH, H.J. (1993) Magma ocean formation due to giant impacts. *Journal of Geophysical Research* 98, 5319–5333.

WANG, K., MOYNIER, F., DAUPHAS, N., BARRAT, J.-A., CRADDOCK, P., SIO, C.K. (2012) Iron isotope fractionation in planetary crusts. *Geochimica et Cosmochimica Acta* 89, 302–321.

WILDING, M.C., BENMORE, C.J., TANGEMAN, J.A., SAMPATH, S. (2004) Evidence of different structures in magnesium silicate liquids: coordination changes in forsterite- to enstatite-composition glasses. *Chemical Geology* 213, 281–291.

WOOD, J.A., DICKEY, J.S., MARVIN, U.B., POWELL, B.N. (1970) Lunar anorthosites. *Science* 167, 602–604.

XIAO, Y., TENG, F.-Z., ZHANG, H.-F., YANG, W. (2013) Large magnesium isotope fractionation in peridotite xenoliths from eastern North China craton: Product of melt–rock interaction. *Geochimica et Cosmochimica Acta* 115, 241–261.

YOUNG, E.D., TONUI, E., MANNING, C.E., SCHAUBLE, E., MACRIS, C.A. (2009) Spinel–olivine magnesium isotope thermometry in the mantle and implications for the Mg isotopic composition of Earth. *Earth and Planetary Science Letters* 288, 524–533.

Tracking the formation of magma oceans in the Solar System using stable magnesium isotopes

M. Schiller[1]*, J.A. Dallas[1], J. Creech[2], M. Bizzarro[1], J.A. Baker[3]

Supplementary Information

The Supplementary Information includes:

- Materials and Methods
- Crystallisation Modelling
- Partial Melting Modelling
- Table S-1
- Figure S-1
- Supplementary Information References

Materials and Methods

Samples

Twenty-two eucrites were selected for study. Nineteen of the eucrites were obtained from the NASA Antarctic meteorite collection and the other three are well-characterised and widely available eucrites (Camel Donga, Juvinas and Millbillillie). All of the studied eucrites are non-cumulates, and the majority are brecciated. Some key characteristics of each analysed eucrite are outlined in Table S-1. Both diogenites analysed in this study are unequilibrated pyroxenites. Detailed petrology for both these samples can be found in Barrat *et al.* (2006) and Yamaguchi *et al.* (2011).

1. Centre for Star and Planet Formation, University of Copenhagen, *Øster* Voldgade 5–7, 1350 Copenhagen, Denmark
* Corresponding author (email: schiller@snm.ku.dk)
2. Institut de Physique du Globe de Paris, Université Paris Diderot, CNRS UMR 7154, 75005 Paris, France
3. School of Environment, The University of Auckland, Private Bag 92019, Auckland, New Zealand

Table S-1 Eucrite samples analysed in this study.

Eucrite sample	NASA classification	Weathering grade	Grain size (μm)	Plagioclase: pyroxene	Mineral properties	Description
EET 83227	polymict	B	<10–200	2:3	Pyroxene shows zoning, and fine (<10 μm) exsolution lamallae	Heavily brecciated anhedral pyroxene and plagioclase clasts in a comminuted matrix
EET 87548	Mg-rich	B/C	30–1800	1:2	Pyroxene exsolution lamallae up to 50 μm	Large brecciated pyroxene and plagioclase clasts, with some finer grained areas
LEW 87002	Mg-rich	Ae	100–1500	1:5	No exsolution or zoning	Coarse grained euhedral pyroxene clasts, with areas of ophitic pyroxene–plagioclase intergrowth
Camel Donga	brecciated	-	10–500	2:3	Pyroxene exsolution lamallae <10 μm	Range of rounded and angular grains of pyroxene and plagioclase in a comminuted groundmass of these minerals
EET 92003	brecciated	A/Be	10–200	1:2	No exsolution or zoning	Fine grained aggregate of pyroxene and plagioclase, with few larger brecciated clasts
GRA 98006	brecciated	A/B	10–1000	3:1	Pyroxene exsolution lamallae *ca.* 10 μm	Coarse plagioclase clasts set in brecciated pyroxene
GRA 98033	brecciated	A/B	>1000	1:2	Pyroxene exsolution lamallae up to 100 μm	Coarse, heavily brecciated pyroxene and plagioclase clasts
GRA 98043	brecciated	C	50–500	1:1	Pyroxene exsolution lamallae *ca.* 30 μm	Ophitic intergrowth of elongate euhedral plagioclase clasts and anhedral pyroxene
GRA 98055	brecciated	B	100–500	1:1	Pyroxene exsolution lamallae 10–50 μm	Equigranular intergrowth of euhedral plagioclase and pyroxene
GRA 98114	brecciated	B	<10–500	1:1	Pyroxene exsolution lamallae 10–50 μm	Granular aggregate of pyroxene and plagioclase, with few large pyroxene clasts
GRO 95533	brecciated	A/B	500	2:3	Pyroxene exsolution lamallae *ca.* 10 μm	Coarse-grained brecciated anhedral plagioclase and pyroxene
Juvinas	brecciated	-	500–1000	1:2	Pyroxene exsolution lamallae <10 μm	Granoblastic texture, with euhedral plagioclase grains, with numerous oxide inclusions along grain boundaries
LAP 031062	brecciated	A/B	100–1000	1:10	Pyroxene exsolution lamallae <10 μm	Heavily brecciated subhedral pyroxene clasts with occasional euhedral plagioclase clasts

Eucrite sample	NASA classification	Weathering grade	Grain size (μm)	Plagioclase: pyroxene	Mineral properties	Description
LAR 06875	brecciated	B/C	50–100	2:3	Pyroxene exsolution lamallae <10 μm	Fine grained, cataclastic texture of relatively rounded plagioclase and pyroxene
Millbillillie	brecciated	-	10–500	1:1	Pyroxene exsolution lamallae <10 μm	Ophitic texture, with large plagioclase and pyroxene grains in a comminuted matrix
PCA 91193	brecciated	A/Be	50–500	2:3	Pyroxene exsolution lamallae 10–50 μm	Brecciated subhedral clasts of pyroxene and plagioclase in a comminuted matrix
QUE 99005	brecciated	B	<1000	1:1	No exsolution	Ophitic texture, with large plagioclase and pyroxene grains in a comminuted matrix
RKPA 80204	brecciated	A	<200	1:1	Pyroxene shows zoning and exsolution lamallae <10 μm	Fine grained ophitic texture with larger plagioclase and pyroxene grains in a finer matrix of these minerals
SCO 06041	brecciated	A	10–2000	2:3	Pyroxene exsolution lamallae <10 μm	Large basaltic clasts in a comminuted pyroxene and plagioclase groundmass
EET 92023	unbrecciated	A	1000–2000	2:3	Fine (<10 μm) pyroxene exsolution	Subhedral intergrowth of pyroxene and plagioclase
LEW 85305	unbrecciated	A	500–1000	1:1	Pyroxene exsolution lamallae <10 μm	Subhedral intergrowth of plagioclase and pyroxene, and some areas of granulated pyroxene
QUE 97014	unbrecciated	A	100–300	1:1	Pyroxene exsolution lamallae <50 μm	Anhedral clasts of plagioclase and pyroxene and some areas of granulated pyroxene

Notes: Weathering grade according to the Meteorite Working Group for Antarctic meteorites: (A) minor rustiness; rust haloes on metal particles and rust stains along fractures are minor; (B) moderate rustiness; large rust haloes occur on metal particles and rust stains on internal fractures are extensive; (C) severe rustiness; metal particles have been mostly stained by rust throughout; (e) evaporite minerals visible to the naked eye.

Analytical methods

Samples were lightly crushed in an agate mortar with a pestle and fragments visually free of surficial alteration weighing 100–200 mg were then handpicked for digestion. Given that the maximum grain size in the samples is *ca*. 2 mm, chips of this size are likely to be broadly representative of each sample. The sample chips were rinsed in ethanol and placed in 10 mL of 0.05M HNO_3 in an ultrasonic bath for 5 min for cleaning prior to digestion. The samples were digested, along with the USGS basaltic rock standard BHVO-2 in concentrated HF–HNO_3 (3:1)

at a temperature of 120 ˚C. Following this, samples were refluxed repeatedly in concentrated HNO_3 and HCl acids, before a final reflux in aqua regia, in order to ensure that the samples were completely dissolved. All samples were visually inspected during these latter digestion steps to ensure that no material remained undigested. An aliquot comprising 2.5–5.0 mg of digested sample was processed through a six-step ion exchange procedure for Mg separation. Magnesium was purified from the sample matrices by ion exchange chromatography based on protocols developed in Bizzarro *et al.* (2011). In detail, Mg was separated using a six-step purification scheme that combines cation, anion, TODGA and Ni-spec resins (Bizzarro *et al.*, 2011). This procedure ensures that Mg was efficiently separated from elements that may result in isobaric interferences during isotope measurements, such as ^{48}Ca, ^{48}Ti, ^{50}Ti, ^{50}V, ^{50}Cr and ^{52}Cr, and elements such as Na, Al, Ca, Fe, Ni and Ti, which may affect instrumental mass bias (Bizzarro *et al.*, 2011). This chemical separation process ensures 99.9 % recovery of Mg of a high degree of purity. The full procedural blanks were <15 ng, which are negligible compared to the amount of Mg processed and recovered (>200 μg). The ratios of Na/Mg, Al/Mg, Ca/Mg, Ti/Mg, V/Mg, Cr/Mg and Fe/Mg observed in the separated Mg cuts were typically <0.0001.

The isotopic composition of the purified Mg was determined using a Neptune MC-ICPMS Plus at the Centre for Star and Planet Formation, Natural History Museum of Denmark, and full analytical procedures are reported in Bizzarro *et al.* (2011). The overall analytical protocol applied to the measurement of the eucrites here is the same as that used to measure Mg isotopes for diogenites (Schiller *et al.*, 2011) and the angrite NWA 1670 (Schiller *et al.*, 2015).

Magnesium isotope data were acquired in static mode using three Faraday collectors set-up as follows: ^{26}Mg in the high-3 collector on the high mass side of the axial Faraday, ^{25}Mg in the axial collector, and ^{24}Mg in the low-3 collector on the low mass side of the axial Faraday. The low-3 Faraday collector (^{24}Mg) was connected to an amplifier with a 10^{10} Ω feedback resistor, whereas the axial and high-3 collectors were connected to amplifiers with 10^{11} Ω feedback resistors. Samples were aspirated into the plasma source by means of an Apex sample introduction system with an uptake rate of ~50 μL min^{-1}, and the Mg isotope composition was measured in high-resolution mode ($M/\Delta M > 5000$ as defined by the peak edge width from 5 %–95 % full peak height). Using this approach, the sensitivity of the instrument was ~200 V ppm^{-1} and samples were typically analysed with a signal intensity ranging from 100 V on mass ^{24}Mg and signal intensities of the standard were matched to within 2 % of that of the sample. Single analyses comprised 1667 s of data acquisition consisting of 100 individual 16.67 s integrations and each sample analysis was bracketed by standard analyses. Samples were systematically analysed ten times in this fashion, resulting in the consumption of 10–20 μg of Mg per sample.

Mg isotope data are reported in the μ-notation as relative deviations from the DSM-3 standard according to the following formula

$$\mu^{x}Mg = [(^{x}Mg/^{24}Mg)_{sample} / (^{x}Mg/^{24}Mg)_{DSM\text{-}3} - 1] \times 10^{6} \qquad \text{Eq. S-1}$$

where x represent mass 25 or 26. All Mg data reduction was conducted offline using the freely distributed Iolite data reduction package which runs within Igor Pro (Paton *et al.*, 2011) and changes in mass bias with time were interpolated using a smoothed cubic spline. For each analysis, the mean and standard error of the measured ratios were calculated using a 3 SD threshold to reject outliers. The ten individual analyses of a sample, representing a total of *ca.* 278 min of sample analysis, were combined to produce an average weighted mean using the propagated uncertainties of each individual analysis, and the reported final uncertainties are the 2 SE of the mean of the ten individual sample analyses reported in Table 1. The external reproducibility of our μ^{25}Mg measurements using this method is 20 ppm based on repeated measurements of terrestrial rock standards as well as extraterrestrial materials (Bizzarro *et al.*, 2011).

Crystallisation Modelling

We computed a crystallisation model for parental magmas on Vesta derived from large degrees of partial melting (Ashcroft and Wood, 2015). Crystallisation of 50 %–100 % partial melts in a shallow magma body (at 0.005 GPa) were modelled using the Cobra client of MELTS (Ghiorso and Sack, 1995; Asimow and Ghiorso, 1998) throughout their crystallisation history. In all these models >50 % crystallisation of olivine and orthopyroxene occurs before the residual liquid reaches a MgO content that is comparable to that of the primitive (most magnesian) eucrites.

The evolution of μ^{25}Mg during crystallisation was then modelled by removal of olivine and orthopyroxene from the parental magma with an assumed constant $\mu^{25}Mg_{melt-olivine}$ = +35 ± 10 ppm and $\mu^{25}Mg_{melt-orthopyroxene}$ = +20 ± 10 ppm throughout the crystallisation sequence ignoring changes to the fractionation factor due to varying temperatures. We based this stable isotope fractionation between olivine and melt on the upper limit of 35 ppm determined for high temperature fractionation between olivine and terrestrial basalts (Teng *et al.*, 2007), as well as the offset observed between olivine and groundmass in the angrite NWA 1670 and olivine and whole-rocks in Hawaiian basalts (Fig. 2). The stable isotope fractionation between orthopyroxene and melt was based on the theoretical difference between the fractionation factors for olivine–orthopyroxene and olivine–clinopyroxene systems (Huang *et al.*, 2013) and the slightly lower temperatures of the system at which orthopyroxene crystallises as opposed to olivine.

Our models show that only a 35 ± 10 ppm offset in μ^{25}Mg between olivine and melt and a 20 ± 10 ppm offset in μ^{25}Mg between orthopyroxene and melt is sufficient to increase the μ^{25}Mg composition of the melt from a value where diogenites formed, to that of the final magma from which eucrites crystallised by a combination of equilibrium and fractional crystallisation of olivine and fractional crystallisation of orthopyroxene. MELTS models were evolved from a bulk primitive vestan mantle (Ashcroft and Wood, 2015) by either equilibrium or fractional crystallisation or a combination thereof from their liquidus temperature in 5 ˚C steps (Figs. 3 and S-1). For starting melts produced at <100 % melting, the

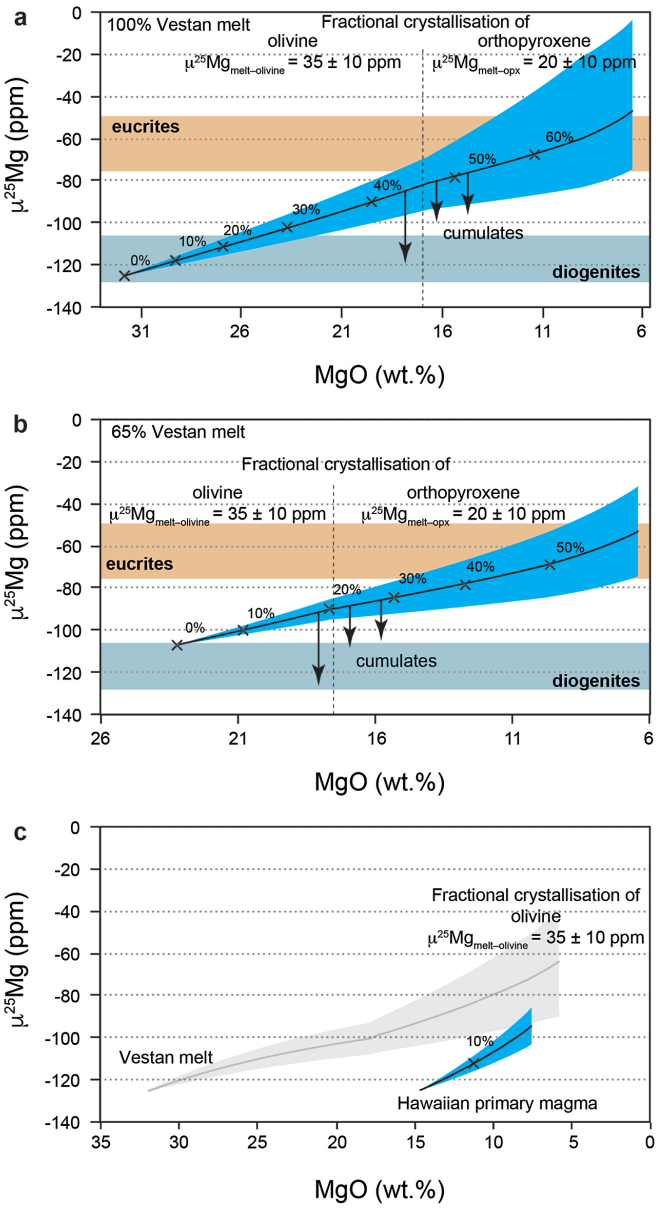

Figure S-1 Shown in **(a)** is the evolution of the μ^{25}Mg of a melt with a composition equivalent to a completely molten vestan mantle (Ashcroft and Wood, 2015) during fractional crystallisation of olivine and orthopyroxene. The amount of fractional crystallisation of each mineral

phase is in accordance with that predicted by a simulation of the fractional crystallisation using MELTS. In **(b)** a similar evolution is shown starting from a composition after 35 % equilibrium crystallisation of olivine. For comparison, a similar evolution is shown in **(c)** for a putative Hawaiian primary melt.

starting compositions were determined by equilibrium crystallising the melt from the liquidus to the desired amount of residual using MELTS. The μ^{25}Mg evolution of the melt was then calculated based on the mole fraction of Mg crystallised from the melt as olivine or orthopyroxene in each step taking into account the respective α factors.

Figure S-1 shows a number of further models. Firstly, the evolution of μ^{25}Mg during fractional crystallisation of a 100 % partial melt of vestan silicate mantle using a vestan primitive mantle composition (Ashcroft and Wood, 2015). In accordance with the mineralogy predicted by MELTS, this model shows that fractional crystallisation of 45 % olivine and *ca.* 25 % orthopyroxene also produces a residual melt with a MgO and μ^{25}Mg composition in the range of eucrites. However, resulting orthopyroxene compositions are predicted to be slightly heavier than observed for diogenites. Combined with the fact that this model results in a slightly higher μ^{25}Mg than the mean composition determined for eucrites either implies that it overestimates the initial degree of melting, isotopic fractionation between minerals and melt, or that not all crystallisation was fractional (*i.e.* Rayleigh) in nature. The second model (Fig. S-1b) starts with a melt composition identical to a 100 % vestan primitive mantle melt after 35 % equilibrium crystallisation of olivine (Fig. 3). In this model, the mode of olivine crystallisation is then changed from equilibrium to fractional crystallisation. This model demonstrates that fractional crystallisation of olivine followed by orthopyroxene from a lower degree partial melt on Vesta is also able to produce a residual melt with a MgO and μ^{25}Mg composition in the range of eucrites and cumulates with μ^{25}Mg compositions of diogenites.

The model shown in Figure S-1c illustrates the MgO and μ^{25}Mg evolution of a primary Hawaiian melt in comparison to that of the 100 % vestan melt shown in Figure 3. The starting MgO content for the Hawaiian model is based on analyses of the primitive glasses (*i.e.* melts) measured in Hawaiian samples, and using data for sample KI88-1-165.0 from the Kilaeau Iki lava lake (Helz and Taggart Jr., 2010). Only a small change in μ^{25}Mg (<40 ppm) is generated in the residual melt by fractional crystallisation of olivine until other phases (pyroxene and feldspar) join the fractionating assemblage. This demonstrates one of the reasons why magmatically driven Mg isotopic fractionations have yet to be clearly detected in cogenetic terrestrial magmas.

Partial Melting Modelling

Minimum estimates of the degree of melting of the vestan silicate mantle were made using analyses of incompatible trace elements in diogenite pyroxene made by laser ablation inductively coupled plasma mass spectrometry (Schiller *et al.*, 2011) or on acid leached residues of diogenites that are inferred to represent pyroxene analyses (Barrat *et al.*, 2010). The degree of partial melting was estimated as follows:

1. Trace element data was compiled from primitive diogenites with the largest μ^{26}Mg* deficits (Schiller *et al.*, 2011), which indicate they are the oldest diogenites. These diogenites also have rare earth element ratios (REE; *e.g.*, Dy/Yb), which indicate they crystallised from a melt with broadly chondritic REE ratios.
2. The elements Y, Dy, Yb, Zr and Hf were selected for modelling given they are present in measurable concentrations in the diogenite pyroxenes, are moderately to highly incompatible during partial melting, have relatively well constrained pyroxene–melt partition coefficients, and are largely immobile during weathering.
3. The pyroxene trace element concentrations were inverted to equilibrium melt compositions using published mineral–melt partition coefficients (Y = 0.065; Dy = 0.05; Yb = 0.1; Zr = 0.023; Hf = 0.04; van Kan Parker *et al.*, 2010).
4. The equilibrium melt compositions were modelled to represent partial melting of vestan silicate mantle with a trace element concentration modified by removing the 16 % mass of the vestan core (Ashcroft and Wood, 2015) from a CI chondrite composition (Palme *et al.*, 2014). By assuming each element is perfectly incompatible a model degree of partial melting can be calculated for each sample and element using simplified expressions of either equilibrium batch or accumulated fractional melting where

$$\text{Percent melting} = 100 \times (X_{BSV}/X_{melt}) \text{ when } D = 0 \qquad \text{Eq. S-2}$$

where X = the element concentration in bulk silicate Vesta (*i.e.* its initial mantle) or diogenite parental melt, and D is the bulk distribution coefficient of element X during mantle melting.

Although the results show some scatter (Fig. 1), most samples and elemental concentrations are best modelled as being ≥40 % partial melting. Although the assumption that these elements are perfectly incompatible during partial melting is not necessarily realistic, it is broadly consistent with the inferred clinopyroxene-free source of vestan magmas (Barrat and Yamaguchi, 2014). Moreover, if the calculations are conducted with non-zero partition coefficients, then the modelled degrees of partial melting increase further. Similarly, the parental magmas of these primitive diogenites may have already experienced some crystallisation and incompatible trace element enrichment prior to diogenite crystallisation. As such, our approach almost certainly underestimates the degree of partial melting of the vestan silicate mantle.

Supplementary Information References

Ashcroft, H.O., Wood, B.J. (2015) An experimental study of partial melting and fractional crystallisation on the HED parent body. *Meteoritics and Planetary Science* 48, 2333–2349.

Asimow, P.D., Ghiorso, M.S. (1998) Algorithmic modifications extending MELTS to calculate subsolidus phase relations. *American Mineralogist* 83, 1127–1131.

Barrat, J.A., Yamaguchi, A. (2014) Comment on "The origin of eucrites, diogenites, and olivine diogenites: Magma ocean crystallisation and shallow magma processes on Vesta" by B.E. Mandler and L.T. Elkins-Tanton. *Meteoritics and Planetary Science* 49, 468–472.

Barrat, J.A., Beck, P., Cotton, J., Gillet, P.H., Greenwood, R.C., Franchi, I.A. (2006) Petrology and geochemistry of the fine-grained, unbrecciated diogenite Northwest Africa 4215. *Meteoritics and Planetary Science* 41, 1045–1057.

Barrat, J.A., Yamaguchi, A., Zanda, B., Bollinger, C., Bohn, M. (2010) Relative chronology of crust formation on asteroid Vesta: Insights from the geochemistry of diogenites. *Geochimica et Cosmochimica Acta* 74, 6218–6231.

Bizzarro, M., Paton, C., Larsen, K., Schiller, M., Trinquier, A., Ulfbeck, D. (2011) High-precision Mg-isotope measurements of terrestrial and extraterrestrial material by HR-MC-ICPMS —Implications for the relative and absolute Mg-isotope composition of the bulk silicate Earth. *Journal of Analytical Atomic Spectrometry* 26, 565–577.

Ghiorso, M.S., Sack, R.O. (1995) Chemical mass transfer in magmatic processes. IV. A revised and internally consistent thermodynamic model for the interpolation and extrapolation of liquid-solid equilibria in magmatic systems at elevated temperatures and pressures. *Contributions to Mineralogy and Petrology* 119, 197–212.

Helz, R.T., Taggart Jr., J.E. (2010) Whole-rock analyses of core samples from the 1988 drilling of Kilauea Iki lava lake, Hawaii. *U.S. Geological Survey Open-File Report* 2010–1093, 47 p.

Huang, F.L. Chen, L., Wu, Z., Wang, W. (2013) First-principles calculations of equilibrium Mg isotope fractionations between garnet, clinopyroxene, orthopyroxene, and olivine: Implications for Mg isotope thermometry. *Earth and Planetary Science Letters* 367, 61–70.

Palme, H., Lodders, K., Jones, A. (2014) Solar System abundances of the elements. In: Holland, H., Turekian, K. (Eds.) *Treatise on Geochemistry*. 2nd Edition, Elsevier, Amsterdam, Netherlands, 455p.

Paton, C., Hellstrom, J., Paul, B., Woodhead, J., Hergt, J. (2011) Iolite: Freeware for the visualisation and processing of mass spectrometric data. *Journal of Analytical Atomic Spectrometry* 26, 2508-2518.

Schiller, M., Baker, J.A., Creech, J., Paton, C., Millet, M.-A., Irving, A., Bizzarro, M. (2011) Rapid timescales for magma ocean crystallisation on the howardite–eucrite–diogenite parent body. *Astrophysical Journal Letters* 740, L22.

Schiller, M., Connelly, J.N., Glad, A.C., Mikouchi, T., Bizzarro, M. (2015) Early accretion of protoplanets inferred from a reduced inner solar system ^{26}Al inventory. *Earth and Planetary Science Letters* 420, 45–54.

Teng, F.-Z., Wadhwa, M., Helz, R.T. (2007) Investigation of magnesium isotope fractionation during basalt differentiation: Implications for a chondritic composition of the terrestrial mantle. *Earth and Planetary Science Letters* 261, 84–92.

van Kan Parker, M., Liebscher, A., Frei, D., van Sijl, J., van Westrenen, W., Blundy, J., Franz, G. (2010) Experimental and computational study of trace element distribution between orthopyroxene and anhydrous silicate melt: substitution mechanisms and the effect of iron. *Contributions to Mineralogy and Petrology* 159, 459–473.

Yamaguchi, A., Barrat, J.-A., Ito, M., Bohn, M. (2011) Posteucritic magmatism on Vesta: Evidence from the petrology and thermal history of diogenites. *Journal of Geophysical Research* 116, 2156-2202.